Melt Morphology of Polystyrene−Poly(ethylene oxide) Metallo-Supramolecular Diblock Copolymer

M. Al-Hussein,[†] B. G. G. Lohmeijer,[‡] U. S. Schubert,[‡] and W. H. de Jeu*[,†]

FOM-Institute for Atomic and Molecular Physics, Kruislaan 407, 1098 SJ Amsterdam, The Netherlands, and Laboratory of Macromolecular Chemistry and Nanoscience and The Dutch Polymer Institute, Eindhoven University of Technology, PO Box 513, 5600 MB Eindhoven, The Netherlands

Received August 12, 2003

Revised Manuscript Received October 29, 2003

Introduction. The capability of block copolymers to self-assemble into nanoscale structures makes them of great importance in the field of nanotechnology. Conventional block copolymers are composed of two or more chemically distinct macromolecules which are linked together through covalent bonds.[1,2] Recently, some of us have developed a new strategy to synthesize block copolymers that combines both supramolecular and polymer chemistry.[3] In this scheme, a metal−ligand complex is used as a supramolecular linker between the different macromolecules of the copolymer. This gives rise to metallo-supramolecular block copolymers that offer several advantages compared with their conventional counterparts. The reversibility of the supramolecular bond potentially allows an improved control of the material properties. Moreover, the presence of a metal complex in the copolymer structure introduces additional electrochemical, photochemical, and redox properties. Generally, the incorporation of inorganic nanoparticles in block copolymers holds the potential of creating new materials such as high-density nanomagnetic materials or photonic crystals.[4,5] Most of the attempts in this direction rely on chemical or physical interactions between one of the blocks and the inorganic particle. This, usually, requires the synthesis of a special block copolymer. In the case of metallo-supramolecular block copolymers, however, the metal ion is an integral part of the polymer chain itself.

Conventional AB diblock copolymer melts are well understood. They can self-assemble into a series of periodic A and B microdomains with a 10−100 nm period depending on both the strength of the repulsive interaction between the A and B blocks and their composition.[1] The geometry of these domains is largely determined by a delicate balance between the interfacial tension at the domain interface and the stretching energy. Examples of the resulting morphologies include cubically packed spheres, hexagonally packed cylinders, lamellae, and bicontinuous structures. Other factors such as the molecular architecture or additional inter- or intramolecular interactions may contribute to the final melt morphology, too.[6] Therefore, the presence of a charged metal−ligand complex (MLC) in the chains of the metallo-supramolecular diblock copolymer might affect its morphology and lead to different morphologies from those normally observed in their conventional counterparts.

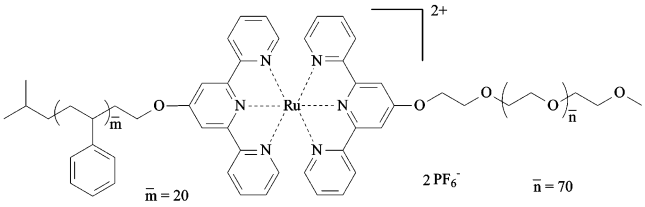

Figure 1. Structure of the PS_{20}-[Ru]-PEO_{70} block copolymer. The numbers in the subscript indicate the degree of polymerization.

In this Communication, we report first results of a small-angle X-ray scattering (SAXS) study of the melt morphology of one of such metallo-supramolecular diblock copolymers, namely metallo-supramolecular polystyrene-*b*-poly(ethylene oxide).

Experimental Section. The synthesis of the polymer used in this study has been described in detail previously.[7] Terpyridine-terminated poly(ethylene oxide) (PEO) and polystyrene (PS) precursors were prepared first. This was demonstrated by ^{1}H NMR, ^{13}C NMR, UV/vis, gel permeation chromatography (GPC), and MALDI−TOF MS measurements. The terpyridine-terminated PEO precursor was then complexed with $RuCl_3$ to form the corresponding monocomplex. Finally, the monocomplex of the terpyridine-terminated poly(ethylene oxide) was reacted with the terpyridine-terminated PS, resulting in the PS_{20}-[Ru]-PEO_{70} metallo-supramolecular copolymer with a polydispersity of 1.10. The chloride counteranions have been exchanged with hexafluorophosphate counteranions to enhance solubility in organic solvents and for comparison with model complexes. Figure 1 shows the chemical structure of the resulting polymer.

Small-angle X-ray scattering (SAXS) measurements were conducted using an in-house setup with a rotating anode X-ray generator (Rigaku RU-H300) operating at 18 kW. By employing two parabolic multilayer mirrors (Bruker, Karlsruhe), a highly parallel beam of a monochromatic Cu Kα radiation (λ = 0.154 nm) with a divergence of 0.012° was obtained. Scattering patterns were recorded using an area detector (Bruker Hi-Star) at a sample-to-detector distance of 1.05 m. The two-dimensional scattering patterns were radially integrated, corrected for the background, and then displayed as one-dimensional plots of the intensity as a function of the modulus q of the scattering vector with $q = (4\pi/\lambda)\sin\theta$, where θ is half the scattering angle.

Results and Discussion. SAXS measurements were used to probe the melt morphology of the PS_{20}-[Ru]-PEO_{70} metallo-supramolecular block copolymer. Figure 2 shows a typical SAXS curve of its melt at 55 °C. The collection time was chosen in a way that few hundreds to around 1000 counts were collected at each angular position, giving a statistical error of 3−8%. The main features of the SAXS curve are a broad peak at about 1.1 nm^{-1} together with an upturn near $q = 0$. Further annealing of the melt up to 2 days did not result in any change in the shape of the SAXS curve. Figure 3 shows a series of SAXS curves at different temperatures. Evidently, the shape of the SAXS curve remains almost the same, and the broad peak persists even at high

[†] FOM-Institute for Atomic and Molecular Physics.
[‡] Eindhoven University of Technology.

10.1021/ma035183z CCC: $25.00
Published on Web 11/15/2003

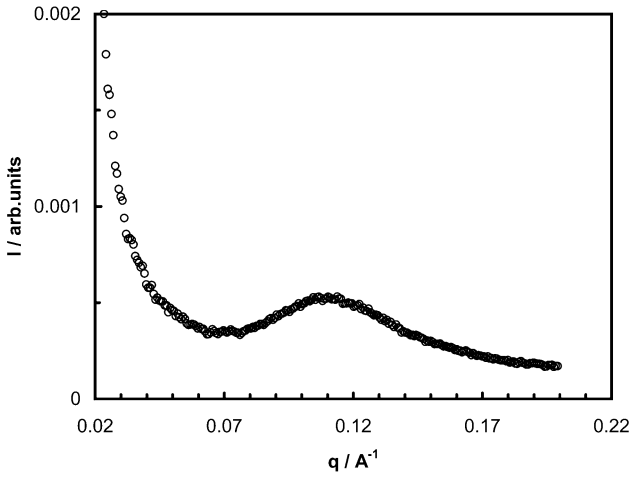

Figure 2. SAXS curve of the PS_{20}-[Ru]-PEO_{70} melt at 55 °C.

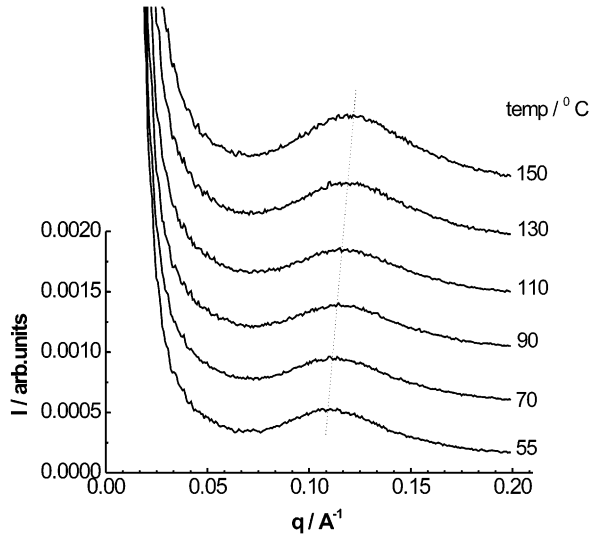

Figure 3. SAXS curve of the PS_{20}-[Ru]-PEO_{70} melt at the temperatures indicated. The dashed line connects the peak positions at different temperatures.

temperatures, although its peak shifts slightly to larger q values. For a conventional diblock copolymer (PS_{22}-*b*-PEO_{70}) with a comparable molecular weight and composition (volume fraction 42% PS), we observed no microphase separation in the melt: its SAXS curve looks featureless. It is known that for such a low molecular weight diblock copolymer microphase separation is inhibited because of the large entropic forces arising from stretching the chains of the two blocks. However, for similar volume fractions (around 42% PS and 58% PEO) but higher molecular weight, microphase separation takes place and the melt exhibits a lamellar morphology.[8] In this case, the SAXS curve shows peaks at $q = nq^*$ where n is an integer and q^* is the scattering vector corresponding to the lamellar period.

The broad peak in the SAXS curve of PS_{20}-[Ru]-PEO_{70} that hardly changes at higher temperatures indicates that the melt morphology is different from its conventional counterpart. Two questions arise here: first, what is the morphological origin of the broad peak? Second, what might be the reason behind the absence of a lamellar phase? It seems natural that any explanation for the difference in morphology between the PS_{20}-[Ru]-PEO_{70} and its nonmetallo counterpart should flow from the presence of the charged MLC in its chains. The difference in polarity between the MLC and the PS and PEO blocks adds an additional driving force to the enthalpic and entropic forces already present. From this point of view, the MLC can be thought of as a third block and correspondingly PS_{20}-[Ru]-PEO_{70} as a triblock copolymer. Triblock copolymers with relatively short minority blocks form spherical domains in their melt.[9,10] Therefore, it is conceivable that the difference in polarity, introduced by the MLC as a "minority block", will trigger off the microphase separation, while the interplay between the various driving forces determines the final morphology of the metallo diblock copolymer melt.

The behavior described thus far shows some parallels with the situation in ionomers, whereby an additional driving force plays a primary role in determining the final morphology.[11,12] Ionomers are ion-containing polymers, consisting of a polymeric backbone with a relatively small number of monomer units with an ionic functionality. Because of the large difference in polarity, the ionic groups tend to form phase-separated ionic aggregates in the hydrophobic matrix. Typically, the SAXS curves of the ionic aggregates show a single broad peak (ionic peak) at 1−4 nm^{-1} and in some cases a strong upturn at low q values.[12] The SAXS curve of Figure 2 shows a striking similarity with this situation. Therefore, it seems reasonable to interpret its broad peak in terms of some aggregations of the MLC ions in the melt. The interaction between ions and counterions groups drives them to form microphase-separated aggregates. This aggregation leads to inevitable unfavorable mixing as well as stretching of the PS and PEO blocks. Apparently, the gain in energy for aggregation overweighs both the enthalpic penalty of mixing and the restoring entropic forces arising from stretching the two blocks. This is in line with the absence of experimental indications of a lamellar microphase.

To quantify the SAXS data, we analyzed the curve of Figure 2 using existing models for ionomers. Several structural models have been proposed to interpret the observed ionic peak in terms of size, shape, and spatial distribution of the ionic aggregates. Essentially all of these models can produce a single broad peak, and therefore it is difficult to distinguish them. They can be divided into two categories: intraaggregate and interaggregate interference models. To asses the applicability of these models to the SAXS curve of Figure 2, we fitted it to a typical model of each category. As a representative for the intraaggregate models, we chose the core−shell model proposed by MacKnight et al.[13] This is a single particle scattering model that attributes the ionic peak to the interference from isolated ionic cores and surrounding shells of ionic pairs. Assuming that the ionic core has a radius R_1 and an electron density difference ρ_1, relative to the hydrocarbon matrix, the inner and outer radii of the shell, with electron density difference ρ_2, are R_2 and R_3, respectively, and the scattered intensity I can be given by

$$I(q) = I_e N \rho_2^2 [V_1 A \Phi(qR_1) + V_3 \Phi(qR_3) - V_2 \Phi(qR_2)]^2 \quad (1)$$

where $\Phi(x) = 3(\sin x - x \cos x)/x^3$, $V_k = (4\pi/3)R_k^3$, and $A = \rho_1/\rho_2$. I_e is the intensity scattered by a single electron under the experimental conditions, and N is the number of aggregates in the scattering volume V. Essentially the shape of the SAXS profile is determined by four

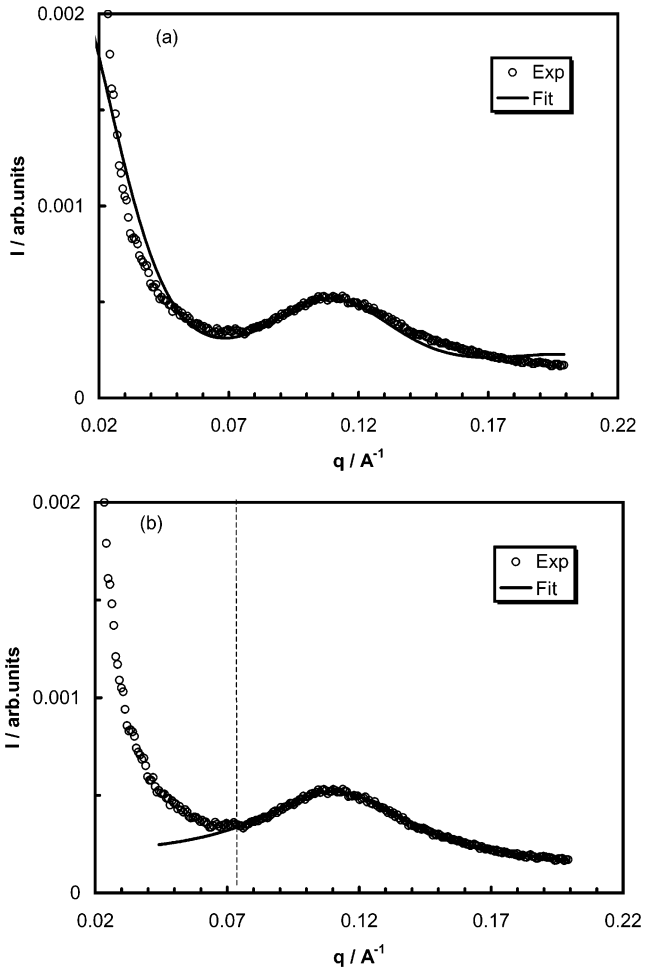

Figure 4. SAXS curve of the PS_{20}-[Ru]-PEO_{70} melt at 55 °C with (a) the fit of the core−shell model and (b) the fit to the Y−C model. The dashed line indicates the lower limit of the fitting range.

parameters: A, R_1, R_2, and R_3. The prefactor $I_e N \rho_2^2$ may be replaced by a single proportionality factor to adjust the intensity scale. Kpl software was used to fit the model to the experimental data.[14] The best-fit values of the parameters were found by a nonlinear least-squares fitting procedure that uses the Levenberg−Marquardt algorithm. The solid line in Figure 4a shows the resulting fit using the core−shell model. The fit resulted in the following parameters: $A = 1.98 \mp 0.12$, $R_1 = 14.52 \mp 0.86$ Å, $R_2 = 67.53 \mp 0.51$ Å, and $R_3 = 68.10 \mp 0.50$ Å. It is evident that the core−shell model is not able to reproduce the whole curve. It provides a fairly good fit in the peak region but fails at low- and high-q regions.

We now turn to the interaggregate models category; as a representative we chose the Yarusso−Cooper (Y−C) model.[15] Evidence from anomalous small-angle X-ray scattering, transmission electron microscopy, and SAXS strongly suggests that this model is the best one to interpret the SAXS data of ionomers.[16−18] The ionic aggregates are considered as spherical particles consisting of an ionic core of radius R_1 and a shell of outer radius R_{ca}. The spheres are dispersed in the polymer matrix with liquidlike order constrained by the distance of closest approach $2R_{ca}$. When applied to PS_{20}-[Ru]-PEO_{70}, the shell layer includes terpyridine ligands and parts of the two block chains as depicted in Figure 5.

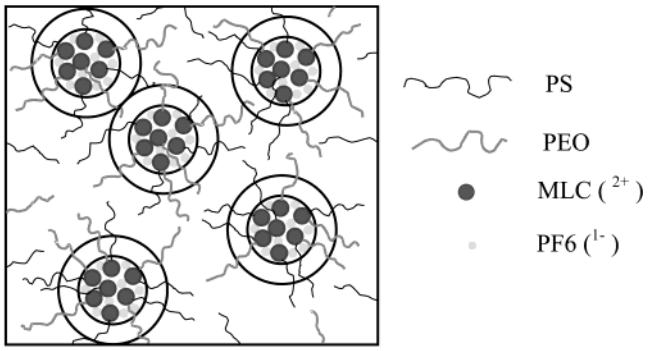

Figure 5. Schematic drawing of the model of the melt morphology of PS_{20}-[Ru]-PEO_{70}. ($^{2+}$) and ($^{1-}$) indicate the charges on each MLC ion and PF_6 counterion, respectively.

Table 1. Best-Fit Parameters for the Y−C Model at Different Temperatures

T/°C	R_1/nm	R_{ca}/nm	V_p/nm^3
55	1.51 ∓ 0.28	2.42 ∓ 0.09	119.9 ∓ 3.6
70	1.50 ∓ 0.27	2.40 ∓ 0.09	119.1 ∓ 3.6
90	1.41 ∓ 0.22	2.31 ∓ 0.08	118.5 ∓ 3.4
110	1.39 ∓ 0.23	2.25 ∓ 0.08	116.6 ∓ 3.6
130	1.35 ∓ 0.23	2.20 ∓ 0.07	109.6 ∓ 3.4
150	1.32 ∓ 0.18	2.16 ∓ 0.05	104.1 ∓ 2.6

According to this model, the scattered intensity is given by

$$I(q) = \frac{I_e N V_1^2 \rho_1^2 \Phi^2(qR_1)}{1 + (8V_{ca}/V_p)\Phi(2qR_{ca})} \qquad (2)$$

I_e, N, $\Phi(x)$, and V_k hold the same definition as above, $V_p = V/N$ is the average sample volume occupied by each aggregate, and ρ_1 is the electron density difference between the ionic cores and the matrix. In this model, the shape of the broad peak is determined by three parameters only: R_1, R_{ca}, and V_p. The only shortcoming of this model is that it fails to predict an upturn in the scattered intensity at low q values. To reproduce the whole curve, a nonrandom long-range distribution of ionic groups and/or ionic aggregates may be added to the Y−C model.[16,18] Here, we restrict ourselves to the analysis of the broad peak only and do not consider any of these modifications. The solid line in Figure 4b represents the resulting fit using the Y−C model for q values in the range 0.73−2 nm^{-1}, which contains the contribution of the broad peak. As can be seen, the model reproduced the peak well. Good fits were also found for all the curves displayed in Figure 3. Table 1 summarizes the best-fit parameters used to reproduce the broad peak together with their uncertainties at the indicated temperatures. Evidently, the Y−C model appears to fit the broad peak of Figure 2 better than the core−shell model.

The volume fraction of the MLC in the PS_{20}-[Ru]-PEO_{70} can be calculated from the respective densities, the number-average molecular weights of the constituting blocks, and the molar mass of a single MLC. For amorphous PS and PEO the densities are 1.04 and 1.10 g/cm^3, respectively, at 55 °C and 0.99 g/cm^3 and 1.02 g/cm^3 at 150 °C.[8] Echegoyen determined the density and the volume of a similar MLC by X-ray analysis and found 1.68 g/cm^3 for the density and a volume $V_{MLC} =$ 0.9 nm^3 at room temperature.[19] We assume the latter two values to be constant over the whole temperature range. The density for the MLC represents an upper

value, since perfect packing of the MLC in the diblock copolymer will be prevented by the bulky substituents on the rings. Consequently, the MLC could take up a larger volume and the actual volume fraction of the MLC may be higher. Actually, molecular mechanics calculations using HyperChem Pro 6.0 already predict a volume of 1.2 nm^3, excluding counterions and substituents on the center ring of the terpyridine ligand. Nevertheless, using the numbers from X-ray crystallography, the volume fractions at 55 °C are 37.6% for PS, 52.8% for PEO, and 9.6% for the MLC, which hardly change at 150 °C: 37.3%, 53.6%, and 9.1%, respectively. If we now assume that the core of the ionic aggregate contains MLC's only, the number of MLC's incorporated in each aggregate can be estimated by calculating the ratio V_1/V_{MLC}. This mounts to about 16 MLC's per aggregate at 55 °C, which is reduced to about 11 at 150 °C. Obviously, the actual number of MLC's has to be less than these values as some part of the chains must also be incorporated in the aggregate core for reasons mentioned before. Taking V_{MLC} from the molecular mechanics calculations, the numbers are reduced to about 12 and 8, respectively, which we still consider to be upper limits. Interestingly, calculating the volume fraction of the MLC core in the total volume of the aggregate (V_1/V_p), one finds a volume fraction of 11.7% and 9.3% at 55 and 150 °C, respectively. These values correlate well with the previously calculated volume fractions of 9.6% and 9.1% for the MLC in the diblock copolymer itself, as described above. The decrease of the radii of the MLC and of the total aggregate with increasing temperature indicates that the region of restricted mobility has become smaller. This may be attributed to reduced expression of electrostatic interactions at higher temperatures.

In summary, we have presented a first SAXS study of the melt morphology of a metallo-supramolecular PS_{20}-[Ru]-PEO_{70} diblock copolymer. The results indicate that the presence of the MLC in the chains leads to a different morphology from that of a conventional counterpart. The electrostatic interaction between the MLC ions and their associated counterions drives them to form aggregates. A liquidlike model of spherical aggregates could fit the broad peak in the SAXS curve well, giving a core radius of about 1.5 nm surrounded by a polymer shell with an outer radius of approximately 2.4 nm. Increasing the melt temperature weakens this interaction, which in turn leads to a decrease of the aggregate size. Our current research focuses on obtaining direct space images of the melt morphology together with studying the change in order of the aggregates upon the crystallization of the PEO block.

Acknowledgment. This work is part of the research program of the "Stichting voor Fundamenteel Onderzoek der Materie (FOM)", which is financially supported by the "Nederlandse Organisatie voor Wetenschappelijk Onderzoek (NWO)". M.A.H. thanks Prof. B. Stühn (Technische Universität Ilmenau) and Dr. L. Li (AMOLF) for helpful discussions and gratefully acknowledges the financial support by the EU-network POLYNANO under Contract HPRN-CT-1999-00151. B.G.G.L. and U.S.S. thank NWO, the Dutch Polymer Institute (DPI), and the Fonds der Chemischen Industrie for funding. We thank Dr. Sunil K. Varshney (Polymer Source Inc.) for providing us with the conventional diblock copolymer. We thank Dr. S. K. Varshney (Polymer Source Inc.) and Dr. W. Stille (Universität Freiburg) for providing us with the conventional diblock copolymer and the Kpl software, respectively.

References and Notes

(1) Bates, F. M.; Fredrickson, G. H. *Annu. Rev. Phys. Chem.* **1990**, *41*, 525.
(2) Hamley, I. W. *The Physics of Block Copolymers*; Oxford: New York, 1998.
(3) (a) Schubert, U. S.; Eschbaumer, C. *Macromol. Symp.* **2001**, *163*, 177. (b) Schubert, U. S.; Eschbaumer, C. *Angew. Chem.* **2002**, *41*, 2892.
(4) Lopes, W. A. *Phys. Rev. E* **2002**, *65*, 031606.
(5) Bockstaller, M. R.; Kolb, R.; Thomas, E. L. *Adv. Mater.* **2001**, *13*, 1783.
(6) Klok, H. A.; Lecommandoux, S. *Adv. Mater.* **2001**, *13*, 1217.
(7) Lohmeijer, B. G. G.; Schubert, U. S. *Angew. Chem., Int. Ed.* **2002**, *41*, 3825.
(8) Zhu, L.; Cheng, S. Z. D.; Calhoun, B. H.; Ge, Q.; Quirk, R. P.; Thomas, E. L.; Hsiao, B. S.; Yeh, F.; Lotz, B. *Polymer* **2001**, *42*, 5829.
(9) Adams, J. L.; Quiram, D. J.; Graessley, W. W.; Register, R. A.; Marchand, G. R. *Macromolecules* **1996**, *29*, 2929.
(10) Mai, S.; Mingvanish, W.; Turner, S. C.; Chaibundit, C.; Fairclough, J. P. A.; Heatley, F.; Matsen, M. W.; Ryan, A. J.; Booth, C. *Macromolecules* **2000**, *33*, 5124.
(11) Eisenberg, A., Ed. *Ions in Polymers*; American Chemical Society: Washington, DC, 1980.
(12) Tant, M. R., Mauritz, K. A., Wilkes, G. L., Eds. *Ionomers: Synthesis, Structure, Properties and Applications*; Chapman and Hall: London, 1997.
(13) MacKnight, W. J.; Taggart, W. P.; Stein, R. S. *J. Polym. Symp.* **1974**, *45*, 113.
(14) Stille, W. http://frsl06.physik.uni-freiburg.de/privat/stille/kpl/ 2003.
(15) Yarusso, D. J.; Cooper, S. L. *Macromolecules* **1983**, *16*, 1871.
(16) Ding, Y. S.; Hubbard, S. R.; Hodgson, K. O.; Register, R. A.; Cooper, S. L. *Macromolecules* **1988**, *21*, 1698.
(17) Li, C.; Register, R. A.; Cooper, S. L. *Polymer* **1989**, *30*, 1227.
(18) Williams, C. E.; Russel, T. P.; Jerome, R.; Horrion, J. *Macromolecules* **1986**, *19*, 2877.
(19) Pyo, S.; Pérez-Cordero, E.; Bott, S. G.; Echegoyen, L. *Inorg. Chem.* **1999**, *38*, 3337.

MA035183Z